



Published in final edited form as:

J Glaucoma. 2017 June ; 26(6): 592–601. doi:10.1097/IJG.0000000000000621.

Diagnostic Capability of Peripapillary Retinal Volume Measurements in Glaucoma

Huseyin Simavli, MD^{1,2}, Linda Yi-Chieh Poon, MD^{1,3}, Christian John Que, MD¹, Yingna Liu, BA¹, Mustafa Akduman, BSc¹, Edem Tsikata, PhD¹, Johannes F. de Boer, PhD⁴, and Teresa C. Chen, MD¹

¹Department of Ophthalmology, Harvard Medical School, Glaucoma Service, Massachusetts Eye and Ear Infirmary, Boston, MA. ²Department of Ophthalmology, Pamukkale University, School of Medicine, Denizli, Turkey. ³Department of Ophthalmology, Kaohsiung Chang Gung Memorial Hospital, Chang Gung University College of Medicine, Kaohsiung Taiwan. ⁴Department of Physics and Astronomy, Vrije Universiteit, Amsterdam, The Netherlands.

Abstract

Purpose—To determine the diagnostic capability of spectral domain optical coherence tomography (SD-OCT) peripapillary retinal volume (RV) measurements.

Materials and Methods—A total of 156 patients, 89 primary open angle (POAG) and 67 normal subjects, were recruited. SD-OCT peripapillary RV was calculated for four quadrants using 3 annuli of varying scan circle diameters: outer circumpapillary annuli of circular grids 1, 2, and 3 (OCA1, OCA2, OCA3). Area under the receiver operating characteristic (AUROC) curves and pairwise comparisons of receiver operating characteristic (ROC) curves were performed to determine which quadrants were best for diagnosing POAG. The pairwise comparisons of the best ROC curves for RV and RNFL were performed. The artifact rates were analyzed.

Results—Pairwise comparisons showed that the smaller annuli OCA1 and OCA2 had better diagnostic performance than the largest annulus OCA3 ($p < 0.05$ for all quadrants). OCA1 and OCA2 had similar diagnostic performance, except for the inferior quadrant which was better for OCA1 ($p = 0.0033$). The pairwise comparisons of the best ROC curves for RV and RNFL were not statistically significant. Retinal volume measurements had lower rates of artifacts at 7.4% while RNFL measurements had higher rates at 42.9%.

Conclusion—Peripapillary RV measurements have excellent ability for diagnosing not only glaucoma patients but also a subset of early glaucoma patients. The inferior quadrant of peripapillary annulus OCA1 demonstrated the best diagnostic capability for both glaucoma and early glaucoma. The diagnostic ability of RV is comparable to that of RNFL parameters in glaucoma but with lower artifact rates.

Corresponding author: Teresa C. Chen, MD, Massachusetts Eye and Ear Infirmary, Glaucoma Service, 243 Charles Street, Boston, MA 02114, Fax: (617) 573-3707, Telephone: (617) 573-3674, teresa_chen@meei.harvard.edu.

Disclosure

The other authors do not have any financial closures or conflicts of interest in the design or conduct of the study.

Keywords

glaucoma; optical coherence tomography; peripapillary; retinal nerve fiber layer thickness; retinal thickness

Introduction

Glaucoma is diagnosed by a subjective determination that there is a combination of characteristic optic nerve head (ONH) changes and corresponding visual field defects. Objective quantitative detection of glaucomatous structural changes such as retinal nerve fiber layer (RNFL) thinning and ONH changes is possible with optical coherence tomography (OCT), and OCT has been shown to have better diagnostic accuracy compared to optic disc photographs that are subjectively evaluated by general ophthalmologists.¹ OCT, which was first described by Huang et al,² is one of the most popular methods for non-invasive cross-sectional imaging of ocular structures. Compared to time domain OCT, spectral domain optical coherence tomography (SD-OCT) allows for higher resolution, reduced acquisition time, and better reproducibility.³ Additionally, SD-OCT has the ability to create a three-dimensional (3D) image reconstruction that enables volume measurements of the retina. Currently, retinal volume scans are primarily used for the evaluation of retinal diseases.⁴ For glaucoma evaluation, only macular retinal thickness and volume scans are currently being used.⁵⁻⁸ Peripapillary retinal volume scans are currently not used in the evaluation of glaucoma patients.

Peripapillary RNFL thickness measurements are however available in all commercially available SD-OCT devices and have high diagnostic accuracy for glaucoma detection.⁹ In different SD-OCT studies for glaucoma detection, the best areas under the receiver operator characteristic (AUROC) curves for overall RNFL thickness were between 0.837 and 0.988.^{10, 11} Other OCT parameters with diagnostic capability for glaucoma include ONH parameters (rim area, rim thickness, rim volume, and cup volume), ganglion cell layer thickness, and macular parameters (thickness and volume).^{5-8, 11-16} For both time-domain and SD-OCT, a combination of RNFL and ONH parameters improve the ability to distinguish glaucoma from normal patients.^{17, 18}

Of the various OCT parameters used for glaucoma evaluation, peripapillary RNFL thickness is perhaps the most popular OCT parameter for glaucoma diagnosis and monitoring. However, accurate peripapillary RNFL thickness measurements are more difficult to obtain in glaucoma patients, because glaucoma causes a decrease in RNFL reflectivity, making it difficult for segmentation algorithms to differentiate the normally highly reflective RNFL layer from the underlying tissues.¹⁹ Also, the reliability of RNFL thickness measurements decreases with conditions associated with glaucoma patients, such as peripapillary atrophy (PPA) and myopia. For example, studies have shown that the diagnostic performance of RNFL thickness measurements in glaucoma decreases with PPA.²⁰ In beta zones of PPA atrophy, different retinal layers may be absent.²¹ Therefore, PPA makes it difficult to distinguish the RNFL from the other potentially absent underlying layers, even though the RNFL itself is not affected by PPA.²¹ RNFL thickness measurements are also affected by

myopia, which has been reported to be associated with a false positive diagnosis of glaucoma in up to half of subjects.^{22–25} Because of the aforementioned issues with RNFL thickness measurements and PPA, we hypothesize that peripapillary retinal volume (RV) measurements, which may be more consistently obtained in glaucoma patients, may have better diagnostic capability in glaucoma detection than RNFL thickness measurements.

To our knowledge, this is the first study evaluating the diagnostic potential of peripapillary RV measurements for glaucoma. The aim of this study is to evaluate the diagnostic performance of SD-OCT RV measurements for detecting glaucoma by using AUROC curves, sensitivity, specificity, positive predictive values (PPV), negative predictive values (NPV), positive likelihood ratios (PLR), and negative likelihood ratios (NLR).

Materials and Methods

PARTICIPANTS AND EXAMINATIONS

All study subjects were recruited from the Glaucoma Service at the Massachusetts Eye and Ear Infirmary between January 2009 and July 2013, as part of the prospective SIG (Spectral Domain OCT in Glaucoma) Study which was approved by the Massachusetts Eye and Ear Infirmary institutional review board. Informed consent form was obtained from all the subjects participating in the study. All methods adhered to the tenets of the Declaration of Helsinki for research involving human subjects and the study was conducted in accordance with Health Insurance Portability and Accountability Act regulations. All study subjects underwent a complete eye examination by a glaucoma specialist (T.C.C.), and this included history, visual acuity testing, refraction, Goldmann applanation tonometry, slit-lamp biomicroscopy, gonioscopy, ultrasonic pachymetry, dilated ophthalmoscopy, stereo disc photography (Visucam Pro NM; Carl Zeiss Meditec, Inc.), visual field (VF) testing (Swedish Interactive Threshold Algorithm 24–2 test of the Humphrey visual field analyzer 750i; Carl Zeiss Meditec, Inc.), and volume scans using Spectralis OCT (HRA/Spectralis software version 5.4.8.0, Heidelberg Engineering GmbH, Heidelberg, Germany).

Patients were included if they had a spherical equivalent between -5.0 and $+5.0$ diopters and a best-corrected visual acuity of 20/40 or better. Only patients with reliable VF testing were included, with less than 33% fixation losses, less than 20% false-positives, and less than 20% false-negatives. Patients were excluded if they had discernible congenital anomalies of the anterior chamber, corneal scarring or opacities, severe non-proliferative or proliferative diabetic retinopathy, VF loss attributable to a non-glaucoma condition such as having neurological conditions or taking systemic medications that affected VF, or a dilated pupil diameter of less than 2 mm.

Primary open angle glaucoma patients were defined as having characteristic changes of the ONH with corresponding glaucomatous VF defects present on 2 separate occasions consecutively. A glaucomatous VF defect was defined as 3 or more contiguous test locations in the pattern standard deviation plot that were depressed significantly at the $p < 0.05$ level with at least 1 at the $p < 0.01$ level on the same side of the horizontal meridian and if the VF defect corresponded to the optic nerve appearance, which is the same criteria which was used in one of our previous studies.⁹ VF abnormalities were classified as early(mean

deviation [MD] > -6 decibels [dB]), moderate ($-12 \text{ dB} < \text{MD} \leq -6 \text{ dB}$), or severe ($\text{MD} \leq -12 \text{ dB}$).

Normal subjects were those without ocular disease, except for mild cataract, and those with normal VF test results, as defined by a pattern standard deviation of more than 5% and glaucoma hemifield test results within normal limits.²⁶ A mild cataract is defined as one that does not prevent a clear view of the fundus and does not cause a vision worse than 20/40. If both eyes were eligible for the study, 1 eye was randomly selected by using the RANDBETWEEN (min,max) function in Microsoft® Office Excel 2007.

SPECTRALIS OPTICAL COHERENCE TOMOGRAPHY PERIPAPILLARY RETINAL VOLUME SCAN

After pupillary dilation, all SD-OCT imaging was performed with the Spectralis OCT machine which utilizes an 870-nm superluminescent diode source. Additional details of the SD-OCT technique have been described elsewhere.^{27, 28} Spectralis OCT provides an automatic real-time (ART) function with an eye-tracking system that can increase image quality. With the ART function activated, multiple frames of the same scanning location are obtained. These data then are averaged for noise reduction, and eye-motion artifacts are reduced. As suggested by the manufacturer, scans with signal strength of less than 15dB (range, 0 to 40) were excluded from the analysis.²⁹ In addition, the criteria for determining adequate scan quality were as follows: a clear fundus image with good optic disc visibility before and during image acquisition, overlay of volume scan visible and without interruptions, and a continuous scan pattern without missing or blank areas. The Spectralis OCT software enables volume scans, which are performed with a 20×20 degree field and which were centered on the ONH. Within each 20×20 degree volume scan, 193 horizontal B-scans were taken, and each B-scan consisted of 512 A-lines. All 193 B-scans for each subject were checked for algorithm artifacts and errors.

Analysis of volume scans was performed using the Heidelberg Eye Explorer version 1.7.0.0 (Heidelberg Engineering GmbH, Heidelberg, Germany). The Heidelberg's built-in software automatically segmented the internal limiting membrane and the Bruch's membrane. RV values were generated from the region measured between these two layers. The scan area overlay was lowered to zero, and the circular grid pattern was centered on the ONH by one of the authors (H.S.), who was masked to the subjects' clinical information. The mean RV was generated by the internal program algorithm and was recorded in regions which we define as circumpapillary annuli. Three circular grids of different diameters are used in this study: circular grid 1 with the circle diameters of 1, 2, 3 mm, circular grid 2 with circle diameters of 1, 2.22, 3.45 mm, and circular grid 3 with circle diameters of 1, 3, 6 mm. For this paper, we only analyzed the outer annulus for each of the circular grid scan options (light gray areas in Fig 1), because the inner circular region (dark gray filled circles, Fig 1) and inner annulus (white areas, Fig 1) covered portions of the optic nerve. The outer annuli (light gray areas, Fig 1) were further subdivided by quadrant: superior, temporal, inferior and nasal, and the values were obtained for analysis. Throughout the rest of the paper, the outer circumpapillary annuli (OCA) of circular grids 1, 2 and 3 will be called OCA1, OCA2,

and OCA3, respectively. If parts of OCA1, OCA2 or OCA3 extended outside the 20×20 degree field, these areas were excluded from the final data analysis.

In addition to peripapillary volume scans performed for each subject, the average RNFL thickness values for the overall RNFL thickness (360 degrees), for each 90-degree quadrant (superior, temporal, inferior and nasal), and for each sector (superior-temporal [TS], superior nasal [NS], inferior-temporal [TI], and inferior-nasal [NI]) were recorded from the Spectralis OCT RNFL printouts.

ANALYSIS FOR ARTIFACTS

Several types of artifacts were detected while reviewing 2D RNFL scans and 3D RV scans. Specifically, for 2D RNFL scans, the types of artifacts we detected include misidentification of the anterior and posterior RNFL borders, posterior-vitreous detachment (PVD)-associated artifacts, decentration of the peripapillary scan, poor signal, missing parts, incomplete segmentation, motion artifacts, and cut edge. The definitions of these artifacts were previously described.³⁰ For 3D RV scans, the types of artifacts we detected include misidentification of the anterior and posterior retinal borders, PVD-associated artifacts, missing parts, incomplete segmentation, cut edge, as well as inversion and mirror artifacts, which were not seen in 2D RNFL scans. The definitions of mirror and inversion artifacts were previously described by Han and Jaffe.³¹ When an image had multiple artifacts, it was counted only once. The rates of artifacts were calculated by dividing the total number of images with at least one artifact by the total number of images included. For 2D RNFL scans, each patient had one image, so a total of 156 2D scans were reviewed for artifacts. For 3D RV scans, each patient had a set of 193 images, so a total of 30,108 scans were included.

STATISTICAL ANALYSIS

All of the calculations in this article were performed using MedCalc for Windows, version 11.4.2 (MedCalc Software, Ostend, Belgium). Demographic characteristics of the normal and glaucoma groups were compared using chi-square tests for categorical variables and non-paired 2-tailed Student's *t* tests for continuous variables. Receiver operating characteristic (ROC) curves were created, and areas under the receiver operating characteristic (AUROC) curves were calculated for the retinal volume scans of the 4 quadrants (i.e. superior, temporal, inferior, and nasal) for OCA1, OCA2 and OCA3. Sensitivity, specificity, positive predictive value (PPV), negative predictive value (NPV), positive likelihood ratio (PLR), and negative likelihood ratio (NLR) were calculated. The cut off value for each variable is calculated by the statistical program automatically, depending on the maximum value of the *Youden index (J)* which is equal to the maximum of $[Sensitivity + Specificity - 1]$. This value corresponds with the point on the ROC curve furthest from the diagonal line. Pairwise comparisons of ROC curves were performed to determine which quadrant had better accuracy for the diagnosis of glaucoma. False positive and false negative values were evaluated with respect to the cut-off value. Normal subjects who had RV values smaller than the cut off value were counted as false positives, and POAG patients who had RV values larger than the cut off were counted as false negatives. The effects of PPA on false positive and false negative determinations were calculated by chi-square or Fisher's exact test. Additionally, ROC curves of RNFL thickness were created, and

AUROC curves were calculated for overall, 4 quadrants, and 4 sectors. Pairwise comparisons of ROC curve were performed among the AUROC curves with best performance for RV and RNFL thickness measurements for both all POAG patients and a subset of early POAG patients. In addition, stepwise binary logistic regression was used to evaluate the best combinations of RV, RNFL, and both RV and RNFL (RV-RNFL). AUROC values were calculated for the combinations. Pairwise comparisons of AUROC values for each of the combinations of RV versus RNFL, RV versus (RV-RNFL), and RNFL versus RV-RNFL and for each of the best combinations were performed. Differences were considered significant at p values <0.05.

Results

There were 156 study patients, with 67 normal subjects and 89 POAG subjects, after inclusion and exclusion criteria were applied. Of the 89 POAG subjects, 33 of them had early glaucoma (37.1%), 24 of them had moderate glaucoma (27.0%), and 32 of them had severe glaucoma (36.0%), which represents an equal distribution. Demographics of the study population are shown in Table 1. We notably had excluded 12 patients, who had VF loss attributable to a non-glaucoma condition: 1 subject with lupus and hydroxychloroquine use, 1 subject with a history of optic neuritis, 1 subject with a history of a pituitary tumor, 1 subject with a brain tumor, 5 subjects with histories of retinal vein occlusions, and 3 subjects who had retinal detachment repairs.

All 193 B-scans for each subject were checked for algorithm artifacts and errors, and no segmentation errors were noted for any of the automated RV determinations. For all quadrants of OCA1, OCA2 and OCA3, POAG and early POAG patients had smaller retinal volume values compared to normal patients ($p < 0.05$ for all, Table 2).

When analyzing OCA1 and OCA2, there were no subjects who were excluded due to OCA1 and OCA2 being outside the 20×20 degree field scan area. When analyzing OCA3, 38 of 156 subjects (23.7%) were excluded from the analysis, because the 20×20 degree scan area did not fully cover the blue-ringed area for OCA3 (Fig 1). Twenty-one of these incomplete scanned regions were in the superior quadrant, 24 of them were in the nasal quadrant, 6 of them were in the temporal quadrant, and 3 of them were in the inferior quadrant.

In general, the RV values demonstrated good correlation with VF MD for the superior and inferior quadrants, but this decreased with increasing annulus size (OCA1: Spearman's rho (ρ) = 0.642 and 0.708, respectively; OCA2: ρ = 0.612 and 0.674, respectively; OCA3: ρ = 0.533 and 0.583, respectively, p values all < 0.001). The RV values for OCA1 to OCA3 for the temporal and nasal quadrants in general had lower correlation with the VF MD (ρ = 0.321 ~ 0.545, p values all < 0.001).

AUROC curve values of RV for distinguishing normal patients from POAG and early POAG patients with comparison to the RNFL thickness AUROC values is shown in Table 3 and Table 4, respectively. The highest two AUROC curves of RV for distinguishing between normal and both POAG and early POAG patients were both associated with the inferior region [i.e. inferior OCA1 (0.956, 0.934) and inferior OCA2 (0.936, 0.911)]. Pairwise

comparisons of ROC curves also revealed that inferior OCA1, which was the highest ranked AUROC curve, had statistically better diagnostic performance than other annuli quadrants for both POAG and early POAG patients.

In quadrant-based pairwise comparisons of normal versus POAG patients, the smaller annulus OCA1 had significantly better diagnostic capability than the larger annulus OCA3 for all quadrants ($p_{\text{superior}}=0.0123$, $p_{\text{temporal}}=0.0083$, $p_{\text{inferior}}<0.0001$, $p_{\text{nasal}}=0.0093$). Medium-size annulus OCA2 also had significantly better diagnostic capability than the larger annulus OCA3 for all quadrants ($p_{\text{superior}}=0.0296$, $p_{\text{temporal}}=0.0037$, $p_{\text{inferior}}=0.0005$, $p_{\text{nasal}}=0.0019$). OCA1 had the same diagnostic performance as OCA2 except for the inferior quadrant ($p_{\text{superior}}=0.0628$, $p_{\text{temporal}}=0.3646$, $p_{\text{inferior}}=0.0033$, $p_{\text{nasal}}=0.5299$), where OCA1 had significantly better diagnostic capability than OCA2

In quadrant-based pairwise comparisons of ROC curves of normal versus early POAG patients, although smaller annulus OCA1 had higher AUROC curve values than medium-size annulus OCA2, there were no statistically significant differences between ROC curves except for the inferior quadrant ($p_{\text{superior}}=0.4810$, $p_{\text{temporal}}=0.6764$, $p_{\text{inferior}}=0.0068$, $p_{\text{nasal}}=0.6244$), where OCA1 had significantly better diagnostic capability than OCA2. Comparison of ROC curves for smaller annulus OCA1 and larger annulus OCA3 revealed that the ROC curves for OCA1 and OCA3 were similar, except for the inferior quadrant ($p_{\text{superior}}=0.5002$, $p_{\text{temporal}}=0.0671$, $p_{\text{inferior}}=0.0005$, $p_{\text{nasal}}=0.4645$) where OCA1 had significantly better diagnostic capability than OCA3. After comparing ROC curves of medium-size annulus OCA2 and larger annulus OCA3, OCA2 had significantly better ROC curves than OCA3 for the temporal and inferior quadrants ($p_{\text{temporal}}=0.0312$, $p_{\text{inferior}}=0.0037$), but there were no significant differences between the superior and nasal quadrants ($p_{\text{superior}}=0.6521$, $p_{\text{nasal}}=0.2038$).

The diagnostic performance of RV parameters with RV cut-off values which are associated with the highest sensitivity and specificity values for distinguishing normal versus POAG patients is shown in Table 5, and normal versus early POAG patients is shown in Table 6.

Since PPA has been shown to affect the diagnostic ability of RNFL thickness,¹¹ we evaluated RV images for the presence of PPA, in order to determine if PPA was associated with higher rates of false positive or false negative diagnoses of glaucoma. For smaller annulus OCA1 (Fig 1 left upper and lower), β -zone PPA was detected in 34.0% of patients (53 of 156 subjects). For medium-size annulus OCA2 (Fig 1 middle upper and lower, light gray area), β -zone PPA was detected in 21.2% of patients (33 of 156 patients). There were no patients who had PPA that extended into larger annulus OCA3 (Fig 1 right upper and lower, light gray area). For each of the three scan patterns, a total of 624 quadrants (156 subjects \times 4 quadrants) were analyzed. Table 7 shows the incidence of PPA, and it also demonstrates that PPA does not affect rates of false positives or false negatives for the superior and inferior quadrants. Table 7 shows that PPA was noted in 16.5% (103 of 624) of the OCA1 quadrants. The presence of PPA in OCA1 only significantly increased false positive results and decreased false negative results in the temporal quadrant only (Table 7, $p=0.038$, $p=0.002$). For OCA2, PPA was noted in 8.5% (53 of 624) of quadrants (Table 7).

The presence of PPA was not significantly associated with an inaccurate glaucoma diagnosis for any OCA2 quadrant (Table 7).

The AUROC value (with standard error) for overall RNFL is 0.909 (0.0252) for all POAG patients and 0.899 (0.0320) for early POAG patients. The AUROC values for the quadrant RNFL thickness are shown in Table 3 for all POAG patients, and in Table 4 for early POAG patients.

The best RNFL thickness AUROC curve values were associated with the inferior quadrant and overall RNFL thickness (0.930, 0.909 for all POAG patients; 0.922, 0.899 for early POAG patients). Therefore, inferior and overall RNFL thickness measurements were used for pairwise comparisons with inferior OCA1 and inferior OCA2 RV measurements. When comparing best RNFL to RV parameters for normal versus all POAG patients, pairwise comparisons represented similar diagnostic capability for RNFL and RV parameters [inferior OCA1 RV versus inferior RNFL AUROC curves ($p=0.32$), inferior OCA2 RV versus inferior RNFL ($p=0.83$), inferior OCA1 RV versus overall RNFL ($p=0.09$), inferior OCA2 RV versus overall RNFL ($p=0.73$)].

When comparing best RNFL to RV parameters for normal versus early POAG patients, pairwise comparisons showed similar diagnostic capability for RNFL and RV parameters [inferior OCA1 RV versus inferior RNFL AUROC curves ($p=0.68$), inferior OCA2 RV versus inferior RNFL ($p=0.73$), inferior OCA1 RV versus overall RNFL ($p=0.26$), inferior OCA2 RV versus overall RNFL ($p=0.97$)].

Of the 156 2D RNFL scans analyzed, one for each of the 156 patients, a total of 67 scans had at least one artifact, representing an artifact rate of 42.9%. Of a total of 30,108 3D RV B-scans, a total of 2,223 scans had at least one artifact, representing an artifact rate of 7.4%.

The AUROC values (with standard error) of the best combinations of RV, RNFL, and RV-RNFL were 0.960 (0.0150), 0.940(0.0192), and 0.960 (0.0150) respectively. The pairwise comparisons of ROC curves for RV versus RNFL, RV versus RV-RNFL, and RNFL versus RV-RNFL were not statistically significant ($p=0.14$, $p=0.75$, $p=0.14$ respectively).

Discussion

To the best of our knowledge, this is the first study that evaluates the diagnostic capability of peripapillary RV for POAG. Our study shows that SD-OCT peripapillary retinal volume measurements may be used as a diagnostic tool for differentiating glaucoma from normal patients, because both glaucoma patients and a subset of early glaucoma patients have smaller RV values compared to normal patients.

Best diagnostic potential was found for the inferior quadrants of smaller annulus OCA1 and medium-size annulus OCA2. Consistent with published RNFL studies, the RV quadrants with the best diagnostic capability were, in order, the inferior quadrant, followed by the superior quadrant, the temporal quadrant, and then the nasal quadrant (Table 3 and 4).^{5, 6, 14}

RV measurements closer to the ONH (i.e. OCA1 and OCA2) had better diagnostic capability than regions further from the ONH (i.e. OCA3; Table 3 and 4). This is compatible with the fact that retinal thickness measurements closer to the ONH have an increased proportion of RNFL to total retinal thickness³² and that the RNFL is the retinal layer that is preferentially affected by glaucoma disease. Because volume is directly proportional with the thickness and volume is a product of area and thickness, we believe that the diagnostic performance of RV values is largely dependent on the change in RNFL thickness. Moreover, RNFL thinning affects total RV more as the ONH is approached due to the higher proportion of RNFL around the ONH. For the subset of early glaucoma patients, RV measurements closer to the ONH (i.e. OCA1 and OCA2) also had better diagnostic performance than the more peripheral OCA3 (Table 3 and 4).

In order to compare the diagnostic ability of peripapillary RV with RNFL, we calculated the AUROC curves of RNFL data and made pairwise comparisons of the best parameters for RV (inferior OCA1–2) with the best parameters for RNFL (inferior RNFL and overall RNFL). These comparisons showed that the diagnostic potentials of RV and RNFL were similar ($p > 0.05$ for all). We have previously evaluated the diagnostic capability of peripapillary retinal thickness (RT) in the same group of patients using the same OCA diameters in a recent paper,³³ and found that peripapillary RT parameters were either the same or better than RNFL parameters for diagnosing glaucoma.

The clinical utility of peripapillary RNFL thickness measurements may be limited by high rates of artifacts. Errors in RNFL thickness measurements have been reported to range from 18.0 to 46.7%.^{30, 33–36} Peripapillary 3D RV measurements may have advantages over the traditional 2D RNFL thickness measurements, because RV measurements have lower rates of artifacts (i.e. 7.4% compared to 42.9% in the current study). The higher artifact rates for RNFL thickness measurements may partly be due to the fact that glaucoma causes a decrease in reflectivity of the RNFL, which makes it harder to segment the posterior border of the RNFL. In contrast, the retinal pigment epithelium, or the posterior border of the retina, can be easily segmented in both normal and glaucoma patients. Because the posterior border of the retina may be more consistently accurately segmented in even glaucoma patients, peripapillary 3D RV measurement may provide a novel means to assess glaucomatous structural damage in OCT images. On the other hand, another possible reason for the high artifact rates in RNFL thickness measurements found in the current study (42.9%) may be related to the strict definition we used to define imaging artifacts, which also included decentration of the peripapillary RNFL scan as a type of artifact. In a previous study by our group, as many as 27.8% of peripapillary RNFL scans may contain a decentration artifact, where decentration was strictly defined as being more than 10% off the center of the optic nerve head.³⁰ In contrast, the Asrani et al study, which did not include decentration as a type of artifact, reported a much lower RNFL scan artifact rate of 19.9%,³⁵ compared to the current study's overall artifact rate of 42.9%. Nevertheless, despite the relatively lower rate of artifacts in 3D RV measurements compared to 2D RNFL thickness measurements, we found that RV only demonstrated similar glaucoma diagnostic capability compared to RNFL thickness. Future studies which evaluate the subset of patients with unusable RNFL data but usable RV data would be interesting, as this would better define the

percentage of patients who have unusable RNFL data but usable RV as well as better determine the clinical factors associated with poor RNFL versus RV segmentation.

Another potential advantage of 3D RV over 2D RNFL data is that the diagnostic ability of 3D RV data appears to be less affected by PPA than 2D RNFL data. The accuracy of 2D RNFL thickness measurements has been shown to be affected by PPA.^{20, 34} Since PPA is associated with glaucoma, PPA may be a common potential source of error in OCT RNFL measurements. It is important to understand PPA, which can be divided into two zones, an α - and a β -zone.^{20, 21, 37} In an SD-OCT study of 90 eyes, it was shown that β -zone PPA is always associated with an absence of the retinal pigment epithelium (RPE), Bruch's membrane, and the inner and outer segment photoreceptor layer junction.²¹ Moreover, with β -zone PPA, the external limiting membrane was absent in 85% of subjects, the outer plexiform layer was absent in 34% of patients, the inner plexiform layer was absent in 29% of subjects, and the ganglion cell layer was absent in 27% of subjects.²¹ Although the RNFL itself may not be affected with PPA, the absence of the underlying layers may increase the difficulty in determining the RNFL borders and in measuring RNFL thickness, which therefore decreases the diagnostic capability of the RNFL.^{20, 34} In a study of 28 normal and 78 glaucoma eyes, the AUROC of subjects with PPA was significantly less than the subjects without PPA (0.816/0.944, $p < 0.001$).²⁰ Moreover, PPA increased false positive rates for two SD-OCT devices (Spectralis and Cirrus).³⁴ The absence of the RPE/Bruch's membrane complex in subjects with PPA may also potentially cause inaccuracies in retinal volume measurements. Therefore, we investigated whether the presence of PPA decreased the efficacy of RV as a diagnostic parameter for glaucoma. We tested this hypothesis by analyzing the rates of a false positive or false negative diagnosis, with and without PPA (Table 7). We found that although the diagnostic performance of the temporal quadrant of smaller annulus OCA1 was significantly affected by the presence of PPA, none of the other quadrants for either smaller annulus OCA 1 or medium-size annulus OCA2 were significantly affected by the presence of PPA (Table 7). Our findings are preliminary since the sample size was small, and no quantitative grading of the degree of PPA was attempted. Future larger studies are needed to clarify the precise role and effect of PPA on RV measurements.

There are some limitations to this study. First of all, all of the POAG study patients had VF defects. Since we only evaluated the diagnostic accuracy of peripapillary RV for perimetric glaucoma, further studies are still needed to better evaluate the diagnostic capability of peripapillary RV in pre-perimetric glaucoma. Another limitation is that we may not have adequately assessed the diagnostic potential of the largest size annulus OCA3, because OCA3 data was not included in the study if the annulus extended outside the square scanned area. If this patient data were not excluded and if the scanned area were larger, it is possible that the AUROC curve values for this largest size OCA3 annulus may have been different. However, because our study utilized the current ETDRS Heidelberg retinal thickness software with fixed circular grid sizes, this necessitated exclusion of many OCA3 areas. This highlights the limitation of the machine's built-in software for analyzing regions around the optic nerve and highlights the need for new software specifically designed for 3D glaucoma parameters and not diabetic retinopathy data. To address this issue, our group has currently started working on building customized analytical software that is capable of analyzing the

peripapillary region within annuli of modifiable diameters. A third limitation is that this study did not evaluate the effects of aging and high myopia on peripapillary RV measurements. Future studies evaluating the effects of aging and refraction in a larger group of normal patients would be critical for determining the relationship between RV and these factors.

In conclusion, peripapillary RV has been shown to be potentially useful for detecting both POAG as well as a subset of early POAG patients. The inferior and superior quadrants appear to have the best diagnostic capability for this parameter. The smaller annulus OCA1 and medium-size annulus OCA2 appear to have similar diagnostic ability for all quadrants, except for the inferior quadrant which had better diagnostic potential for OCA1. Compared to OCA1, the medium-size annulus OCA2 appears least affected by the presence of PPA. Although our findings suggest that the diagnostic capability of RV was similar to RNFL thickness, under circumstances where occurrence of artifacts in 2D RNFL scans may be high, such as with glaucoma-associated decreased RNFL reflectivity or with PPA, the use of RV for the diagnosis of glaucoma may be useful.

Acknowledgments

Teresa C. Chen has received funding from the following: American Glaucoma Society Mid-Career Award; Massachusetts Lions Eye Fund; Harvard Catalyst Grant, National Institutes of Health Award #UL 1RR 025758; Fidelity Charitable Fund (Harvard University). Johannes de Boer has the following financial disclosures: Harvard Medical School – Center for Biomedical Optical Coherence Tomography Research and Translation Scientific Advisory Board Chair; Licenses to NIDEK, Inc, Fremont, CA; Terumo Corporation, Tokyo, Japan; and Ninepoint Medical, Cambridge, MA. Huseyin Simavli is supported by TUBITAK (The Scientific and Technological Council of Turkey) 2219.

References

1. Vessani RM, Moritz R, Batis L, et al. Comparison of quantitative imaging devices and subjective optic nerve head assessment by general ophthalmologists to differentiate normal from glaucomatous eyes. *J Glaucoma*. 2009; 18:253–261. [PubMed: 19295383]
2. Huang D, Swanson EA, Lin CP, et al. Optical coherence tomography. *Science*. 1991; 254:1178–1181. [PubMed: 1957169]
3. Wu H, de Boer JF, Chen TC. Reproducibility of retinal nerve fiber layer thickness measurements using spectral domain optical coherence tomography. *J Glaucoma*. 2011; 20:470–476. [PubMed: 20852437]
4. Lammer J, Scholda C, Prunte C, et al. Retinal thickness and volume measurements in diabetic macular edema: a comparison of four optical coherence tomography systems. *Retina*. 2011; 31:48–55. [PubMed: 20683379]
5. Nakatani Y, Higashide T, Ohkubo S, et al. Evaluation of macular thickness and peripapillary retinal nerve fiber layer thickness for detection of early glaucoma using spectral domain optical coherence tomography. *J Glaucoma*. 2011; 20:252–259. [PubMed: 20520570]
6. Schulze A, Lamparter J, Pfeiffer N, et al. Diagnostic ability of retinal ganglion cell complex, retinal nerve fiber layer, and optic nerve head measurements by Fourier-domain optical coherence tomography. *Graefes Arch Clin Exp Ophthalmol*. 2011; 249:1039–1045. [PubMed: 21240522]
7. Kita Y, Kita R, Takeyama A, et al. Ability of optical coherence tomography-determined ganglion cell complex thickness to total retinal thickness ratio to diagnose glaucoma. *J Glaucoma*. 2013; 22:757–762. [PubMed: 22668980]
8. Mori S, Hangai M, Sakamoto A, et al. Spectral-domain optical coherence tomography measurement of macular volume for diagnosing glaucoma. *J Glaucoma*. 2010; 19:528–534. [PubMed: 20164794]

9. Wu H, de Boer JF, Chen TC. Diagnostic capability of spectral-domain optical coherence tomography for glaucoma. *Am J Ophthalmol.* 2012; 153:815–26. e2. [PubMed: 22265147]
10. Moreno-Montanes J, Olmo N, Alvarez A, et al. Cirrus high-definition optical coherence tomography compared with Stratus optical coherence tomography in glaucoma diagnosis. *Invest Ophthalmol Vis Sci.* 2010; 51:335–343. [PubMed: 19737881]
11. Hwang YH, Kim YY. Glaucoma diagnostic ability of quadrant and clock-hour neuroretinal rim assessment using cirrus HD optical coherence tomography. *Invest Ophthalmol Vis Sci.* 2012; 53:2226–2234. [PubMed: 22410556]
12. Mwanza JC, Oakley JD, Budenz DL, et al. Ability of cirrus HD-OCT optic nerve head parameters to discriminate normal from glaucomatous eyes. *Ophthalmology.* 2011; 118:241–248. e1. [PubMed: 20920824]
13. Kotowski J, Folio LS, Wollstein G, et al. Glaucoma discrimination of segmented cirrus spectral domain optical coherence tomography (SD-OCT) macular scans. *Br J Ophthalmol.* 2012; 96:1420–1425. [PubMed: 22914498]
14. Na JH, Sung KR, Baek S, et al. Macular and retinal nerve fiber layer thickness: which is more helpful in the diagnosis of glaucoma? *Invest Ophthalmol Vis Sci.* 2011; 52:8094–8101. [PubMed: 21911590]
15. Sung KR, Na JH, Lee Y. Glaucoma diagnostic capabilities of optic nerve head parameters as determined by Cirrus HD optical coherence tomography. *J Glaucoma.* 2012; 21:498–504. [PubMed: 21637115]
16. Rao HL, Zangwill LM, Weinreb RN, et al. Comparison of different spectral domain optical coherence tomography scanning areas for glaucoma diagnosis. *Ophthalmology.* 2010; 117:1692–1699. 9 e1. [PubMed: 20493529]
17. Wang M, Lu AT, Varma R, et al. Combining information from 3 anatomic regions in the diagnosis of glaucoma with time-domain optical coherence tomography. *J Glaucoma.* 2014; 23:129–135. [PubMed: 22828002]
18. Huang JY, Pekmezci M, Mesiwala N, et al. Diagnostic power of optic disc morphology, peripapillary retinal nerve fiber layer thickness, and macular inner retinal layer thickness in glaucoma diagnosis with fourier-domain optical coherence tomography. *J Glaucoma.* 2011; 20:87–94. [PubMed: 20577117]
19. van der Schoot J, Vermeer KA, de Boer JF, et al. The effect of glaucoma on the optical attenuation coefficient of the retinal nerve fiber layer in spectral domain optical coherence tomography images. *Invest Ophthalmol Vis Sci.* 2012; 53:2424–2430. [PubMed: 22427540]
20. Kim SY, Park HY, Park CK. The effects of peripapillary atrophy on the diagnostic ability of Stratus and Cirrus OCT in the analysis of optic nerve head parameters and disc size. *Invest Ophthalmol Vis Sci.* 2012; 53:4475–4484. [PubMed: 22618588]
21. Lee KY, Tomidokoro A, Sakata R, et al. Cross-sectional anatomic configurations of peripapillary atrophy evaluated with spectral domain-optical coherence tomography. *Invest Ophthalmol Vis Sci.* 2010; 51:666–671. [PubMed: 19850838]
22. Leung CK, Mohamed S, Leung KS, et al. Retinal nerve fiber layer measurements in myopia: An optical coherence tomography study. *Invest Ophthalmol Vis Sci.* 2006; 47:5171–5176. [PubMed: 17122099]
23. Qiu KL, Zhang MZ, Leung CK, et al. Diagnostic classification of retinal nerve fiber layer measurement in myopic eyes: a comparison between time-domain and spectral-domain optical coherence tomography. *Am J Ophthalmol.* 2011; 152:646–653. e2. [PubMed: 21726842]
24. Aref AA, Sayyad FE, Mwanza JC, et al. Diagnostic Specificities of Retinal Nerve Fiber Layer, Optic Nerve Head, and Macular Ganglion Cell-Inner Plexiform Layer Measurements in Myopic Eyes. *J Glaucoma.* 2014; 23:487–493. [PubMed: 23221911]
25. Wang G, Qiu KL, Lu XH, et al. The effect of myopia on retinal nerve fibre layer measurement: a comparative study of spectral-domain optical coherence tomography and scanning laser polarimetry. *Br J Ophthalmol.* 2011; 95:255–260. [PubMed: 20584713]
26. Gordon MO, Kass MA. The Ocular Hypertension Treatment Study: design and baseline description of the participants. *Arch Ophthalmol.* 1999; 117:573–583. [PubMed: 10326953]

27. Chen TC, Cense B, Pierce MC, et al. Spectral domain optical coherence tomography: ultra-high speed, ultra-high resolution ophthalmic imaging. *Arch Ophthalmol*. 2005; 123:1715–1720. [PubMed: 16344444]
28. Cense B, Nassif N, Chen T, et al. Ultrahigh-resolution high-speed retinal imaging using spectral-domain optical coherence tomography. *Opt Express*. 2004; 12:2435–2447. [PubMed: 19475080]
29. Heidelberg Engineering. OCT Acquisition Window1-Overview. Spectralis OCT QuickGuide (software version 5.3). Heidelberg: Heidelberg Engineering; 2010.
30. Liu Y, Simavli H, Que CJ, et al. Patient characteristics associated with artifacts in spectralis optical coherence tomography imaging of the retinal nerve fiber layer in glaucoma. *Am J Ophthalmol*. 2015; 159:565–576. e2. [PubMed: 25498118]
31. Han IC, Jaffe GJ. Evaluation of artifacts associated with macular spectral-domain optical coherence tomography. *Ophthalmology*. 2010; 117:1177–1189. e4. [PubMed: 20171740]
32. Varma R, Skaf M, Barron E. Retinal nerve fiber layer thickness in normal human eyes. *Ophthalmology*. 1996; 103:2114–2119. [PubMed: 9003346]
33. Kim NR, Lim H, Kim JH, et al. Factors associated with false positives in retinal nerve fiber layer color codes from spectral-domain optical coherence tomography. *Ophthalmology*. 2011; 118:1774–1781. [PubMed: 21550120]
34. Leal-Fonseca M, Rebolleda G, Oblanca N, et al. A comparison of false positives in retinal nerve fiber layer, optic nerve head and macular ganglion cell-inner plexiform layer from two spectral-domain optical coherence tomography devices. *Graefes Arch Clin Exp Ophthalmol*. 2014; 252:321–330. [PubMed: 24337431]
35. Asrani S, Essaid L, Alder BD, et al. Artifacts in spectral-domain optical coherence tomography measurements in glaucoma. *JAMA Ophthalmol*. 2014; 132:396–402. [PubMed: 24525613]
36. Moreno-Montanes J, Anton A, Olmo N, et al. Misalignments in the retinal nerve fiber layer evaluation using cirrus high-definition optical coherence tomography. *J Glaucoma*. 2011; 20:559–565. [PubMed: 21336154]
37. Hayashi K, Tomidokoro A, Lee KY, et al. Spectral-domain optical coherence tomography of beta-zone peripapillary atrophy: influence of myopia and glaucoma. *Invest Ophthalmol Vis Sci*. 2012; 53:1499–1505. [PubMed: 22323471]

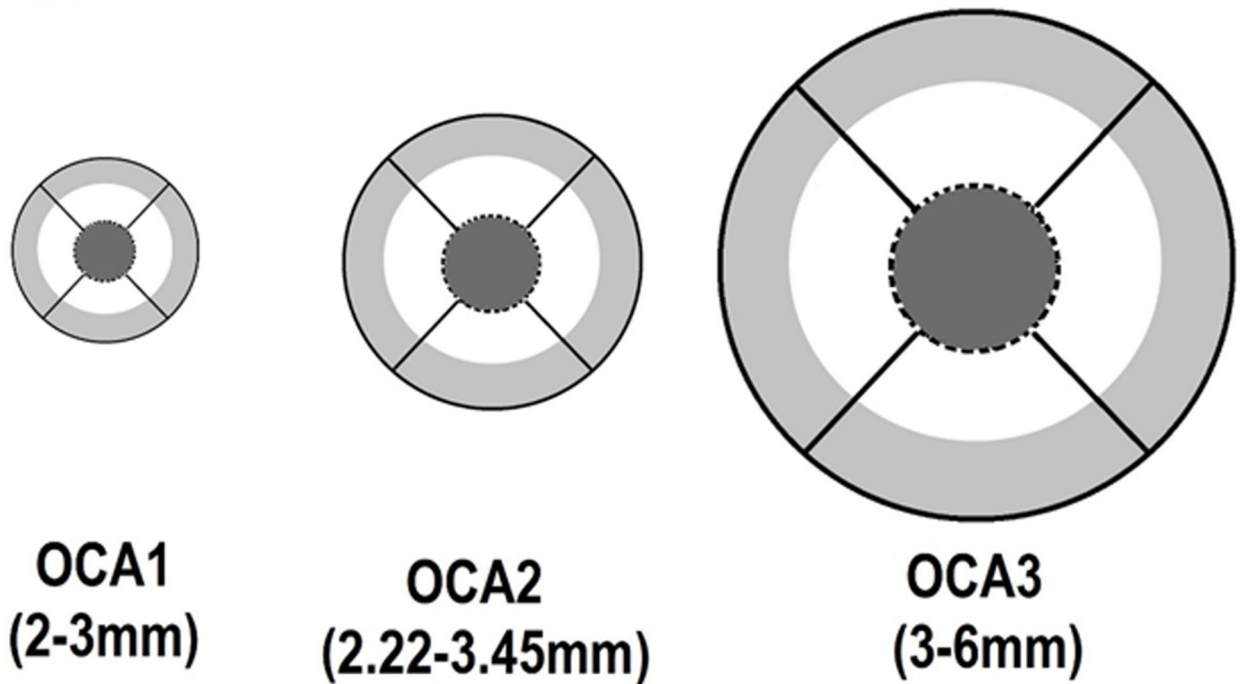
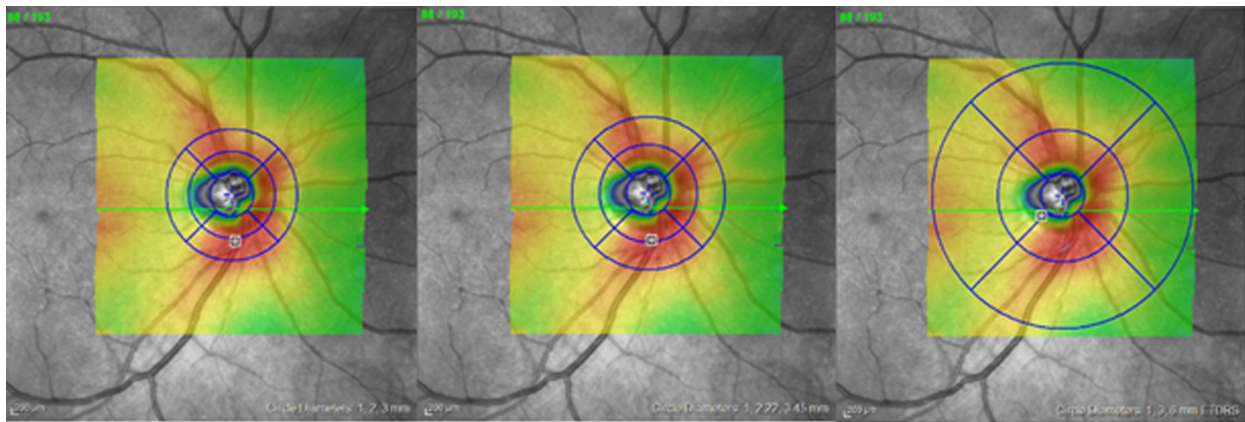


Figure 1. Schematic representation and definition of the outer circumpapillary annuli (OCA1, OCA2, OCA3) of circular grids 1, 2 and 3. The upper row shows the infrared reflectance (IR) images of the optic nerve and peripapillary region. In the IR images, the transparent colored areas which are centered over the optic nerve represent the 20×20 degree region scanned in the 3D volume scan. The blue circular grids are manually centered over the optic nerve from which the machine’s internal software generates the retinal volume values. Images in the lower row shows the diameters of OCA1,2,3 used in this study.

Table 1

Demographics of the normal and primary open angle glaucoma study population

	Normal	POAG	P value*	Early POAG	p value [†]
Number of eyes	67	89		33	
Number of right eyes/left eyes	37/30	51/38	0.871	22/11	0.190
Mean age (years) ± SD	62.6±11.6	66.0±10.6	0.055	67.1±7.9	0.051
Refractive error (D)					
Sphere ± SD	0.008±1.41	0.04±1.23	0.878	-0.19±1.01	0.500
Cylinder ± SD	-0.57±0.74	-0.45±0.81	0.371	-0.74±0.57	0.095
Spherical equivalent ± SD	-0.28±1.52	-0.19±1.18	0.678	1.52±1.01	0.828
VF					
Mean deviation(dB) ± SD	-1.92±1.99	-11.20±7.92	<0.001	-3.97±1.50	<0.001
Pattern standard deviation(dB) ± SD	1.84±0.70	7.01±3.35	<0.001	4.40±1.77	<0.001

POAG: primary open angle glaucoma, SD: standard deviation, D: diopter, dB: decibel, VF: visual field

* Normal patients versus all POAG patients

[†] Normal patients versus a subset of early POAG patients

Table 2

Peripapillary retinal volume measurements for normal and primary open angle glaucoma patients, using 3 circular grids of different diameters.

	Normal Mean±SD (mm³)	POAG Mean±SD (mm³)	Early POAG Mean±SD (mm³)
OCA1			
Superior	0.349±0.046	0.284±0.038 [*]	0.305±0.032 [*]
Temporal	0.302±0.029	0.260±0.033 [*]	0.272±0.033 [*]
Inferior	0.345±0.028	0.272±0.031 [*]	0.287±0.023 [*]
Nasal	0.296±0.028	0.265±0.028 [*]	0.279±0.020 [†]
OCA2			
Superior	0.472±0.061	0.395±0.043 [*]	0.417±0.040 [*]
Temporal	0.417±0.036	0.371±0.036 [*]	0.383±0.037 [*]
Inferior	0.465±0.037	0.381±0.037 [*]	0.397±0.030 [*]
Nasal	0.408±0.034	0.373±0.036 [*]	0.385±0.028 [†]
OCA3			
Superior	1.567±0.124	1.397±0.101 [*]	1.431±0.101 [*]
Temporal	1.532±0.153	1.411±0.130 [*]	1.451±0.146 [§]
Inferior	1.541±0.114	1.351±0.104 [*]	1.385±0.093 [*]
Nasal	1.510±0.158	1.395±0.151 [*]	1.404±0.129 [†]

SD: standard deviation, POAG: primary open angle glaucoma, OCA1: outer circumpapillary annulus of circular grid 1, OCA2: outer circumpapillary annulus of circular grid 2, OCA3: outer circumpapillary annulus of circular grid 3.

^{*} p value comparison to normal < 0.0001;

[†] p value value comparison to normal < 0.01;

[§] p value value comparison to normal < 0.05

Area under the receiver operating characteristic curve of retinal nerve fiber layer thickness and peripapillary retinal volume for normal versus all primary open angle glaucoma patients.

Table 3

	RNFL thickness	Retinal volume (OCA1)	Retinal volume (OCA2)	Retinal volume (OCA3)
	AUROC (SE)	AUROC (SE)	AUROC (SE)	AUROC (SE)
	p value*	p value[†]	p value[‡]	p value[‡]
Superior	0.862 (0.0309)	0.888 (0.0286)	0.878 (0.0298)	0.848 (0.0333)
Temporal	0.821 (0.0366)	0.831 (0.0346)	0.821 (0.0355)	0.728 (0.0418)
Inferior	0.930 (0.0219)	0.956 (0.0181)	0.936 (0.0218)	0.886 (0.0288)
Nasal	0.778 (0.0390)	0.790 (0.0380)	0.758 (0.0402)	0.714 (0.0454)

RNFL: retinal nerve fiber layer, AUROC curve: area under the receiver operating characteristic curve, SE: standard error, OCA1: outer circumpapillary annulus of circular grid 1, OCA2: outer circumpapillary annulus of circular grid 2, OCA3: outer circumpapillary annulus of circular grid 3.

* AUROC of RNFL thickness versus AUROC of retinal volume of OCA1

[†] AUROC of RNFL thickness versus AUROC of retinal volume of OCA2

[‡] AUROC of RNFL thickness versus AUROC of retinal volume of OCA3

Area under the receiver operating characteristic curve of retinal nerve fiber layer thickness and peripapillary retinal volume for normal versus early primary open angle glaucoma patients.

Table 4

	RNFL thickness	Retinal volume (OCA1)	p value *	Retinal volume (OCA2)	p value †	Retinal volume (OCA3)	p value ‡
	AUROC (SE)	AUROC (SE)		AUROC (SE)		AUROC (SE)	
Superior	0.822 (0.0469)	0.807 (0.0463)	0.752	0.805 (0.0465)	0.721	0.800 (0.0455)	0.646
Temporal	0.760 (0.0532)	0.758 (0.0511)	0.970	0.750 (0.0528)	0.853	0.652 (0.0593)	0.061
Inferior	0.922 (0.0295)	0.934 (0.0242)	0.684	0.911 (0.0299)	0.729	0.853 (0.0415)	0.062
Nasal	0.692 (0.0565)	0.701 (0.0518)	0.878	0.698 (0.0533)	0.919	0.711 (0.0592)	0.745

RNFL: retinal nerve fiber layer, AUROC curve: area under the receiver operating characteristic curve, SE: standard error, OCA1: outer circumpapillary annulus of circular grid 1, OCA2: outer circumpapillary annulus of circular grid 2, OCA3: outer circumpapillary annulus of circular grid 3.

* AUROC of RNFL thickness versus Retinal volume of OCA1

† AUROC of RNFL thickness versus Retinal volume of OCA2

‡ AUROC of RNFL thickness versus Retinal volume of OCA3

Diagnostic performance of peripapillary retinal volume for primary open angle glaucoma, with best sensitivity and specificity values for 3 circular grids of different diameters.

Table 5

	Cutoff, mm ³ ()	Sensitivity (CI)	Specificity (CI)	PLR (CI)	NLR (CI)	PPV (CI)	NPV (CI)
OCA1							
Superior	0.32	86.52 (77.6–92.8)	76.12 (64.1–85.7)	3.62 (3.1–4.2)	0.18 (0.09–0.3)	82.8 (73.6–89.8)	81.0 (69.0–89.8)
Temporal	0.28	79.07 (69.0–87.1)	77.61 (65.8–86.9)	3.53 (3.0–4.2)	0.27 (0.1–0.5)	81.9 (71.9–89.6)	74.3 (62.4–84.0)
Inferior	0.31	93.18 (85.7–97.5)	85.07 (74.3–92.6)	6.24 (5.6–7.0)	0.080 (0.03–0.2)	89.1 (80.9–94.7)	90.5 (80.4–96.4)
Nasal	0.29	87.06 (78.0–93.4)	58.21 (45.5–70.2)	2.08 (1.7–2.6)	0.22 (0.1–0.4)	72.5 (62.8–80.9)	78.0 (63.9–88.6)
OCA2							
Superior	0.42	76.40 (66.2–84.8)	86.57 (76.0–93.7)	5.69 (4.9–6.6)	0.27 (0.1–0.6)	88.3 (78.9–94.5)	73.4 (62.3–82.7)
Temporal	0.39	77.65 (67.3–86.0)	76.12 (64.1–85.7)	3.25 (2.7–3.9)	0.29 (0.2–0.5)	80.5 (70.3–88.4)	72.9 (60.9–82.8)
Inferior	0.42	88.64 (80.1–94.4)	88.06 (77.8–94.7)	7.42 (6.6–8.3)	0.13 (0.05–0.3)	90.7 (82.4–95.9)	85.5 (74.9–92.9)
Nasal	0.39	77.65 (67.3–86.0)	62.69 (50.0–74.2)	2.08 (1.7–2.6)	0.36 (0.2–0.60)	72.5 (62.1–81.4)	68.9 (55.7–80.1)
OCA3							
Superior	1.53	91.57 (83.4–96.50)	63.64 (50.9–75.1)	2.52 (2.1–3.1)	0.13 (0.06–0.3)	76.0 (66.4–84.0)	85.7 (72.8–94.10)
Temporal	1.42	59.30 (48.2–69.8)	76.12 (64.1–85.7)	2.48 (2.0–3.1)	0.53 (0.3–0.9)	76.1 (64.1–85.7)	59.3 (48.1–69.8)
Inferior	1.46	84.27 (75.0–91.1)	79.10 (67.4–88.1)	4.03 (3.5–4.7)	0.20 (0.1–0.4)	84.3 (75.0–91.1)	79.1 (67.4–88.1)
Nasal	1.43	68.49 (56.6–78.9)	70.00 (56.8–81.2)	2.28 (1.8–2.9)	0.45 (0.3–0.8)	73.5 (61.4–83.5)	64.6 (51.8–76.1)

CI: 95% confidence interval, PLR: positive likelihood ratio, NLR: negative likelihood ratio, PPV: positive predictive value, NPV: negative predictive value, OCA1: outer circumpapillary annulus of circular grid 1, OCA2: outer circumpapillary annulus of circular grid 2, OCA3: outer circumpapillary annulus of circular grid 3.

Diagnostic performance of peripapillary retinal volume for early primary open angle glaucoma, with best sensitivity and specificity values for 3 circular grids of different diameters.

Table 6

	Cutoff, mm ³ ()	Sensitivity (CI)	Specificity (CI)	PLR (CI)	NLR (CI)	PPV (CI)	NPV (CI)
OCA1							
Superior	0.33	81.82 (64.5–93.0)	65.67 (53.1–76.8)	2.38 (1.9–3.0)	0.28 (0.1–0.6)	54.0 (39.3–68.2)	88.0 (75.5–95.5)
Temporal	0.28	63.64 (45.1–79.6)	77.61 (65.8–86.9)	2.84 (2.1–3.8)	0.47 (0.2–0.9)	58.3 (40.8–74.5)	81.2 (69.5–89.9)
Inferior	0.31	90.91 (75.7–98.1)	85.07 (74.3–92.6)	6.09 (5.3–7.1)	0.11 (0.03–0.4)	75.0 (58.8–87.3)	95.0 (86.0–99.0)
Nasal	0.29	75.76 (57.7–88.9)	58.21 (45.5–70.2)	1.81 (1.4–2.4)	0.42 (0.2–0.8)	47.2 (33.2–61.5)	83.0 (69.2–92.4)
OCA2							
Superior	0.42	63.64 (45.1–79.6)	86.57 (76.0–93.7)	4.74 (3.6–6.2)	0.42 (0.2–0.9)	70.0 (50.6–85.3)	82.9 (71.9–90.9)
Temporal	0.41	81.82 (64.5–93.0)	58.21 (45.5–70.2)	1.96 (1.5–2.5)	0.31 (0.1–0.7)	49.1 (35.2–63.1)	86.7 (73.0–95.0)
Inferior	0.43	87.88 (71.8–96.6)	82.09 (70.8–90.4)	4.91 (4.1–5.8)	0.15 (0.05–0.4)	70.7 (54.5–83.9)	93.2 (83.5–98.1)
Nasal	0.39	69.70 (51.3–84.4)	62.69 (50.0–74.2)	1.87 (1.4–2.5)	0.48 (0.3–0.9)	47.9 (33.3–62.8)	80.8 (67.5–90.4)
OCA3							
Superior	1.55	93.33 (77.9–99.2)	59.09 (46.3–71.0)	2.28 (1.8–2.8)	0.11 (0.03–0.4)	50.9 (37.1–64.6)	95.1 (83.3–99.4)
Temporal	1.42	51.52 (33.5–69.2)	76.12 (64.1–85.7)	2.16 (1.5–3.1)	0.64 (0.4–1.1)	51.5 (33.5–69.2)	76.1 (64.1–85.7)
Inferior	1.42	78.79 (61.1–91.0)	83.58 (72.5–91.5)	4.80 (3.9–5.9)	0.25 (0.1–0.6)	70.3 (53.0–84.1)	88.9 (78.3–95.5)
Nasal	1.43	75.86 (56.5–89.7)	70.00 (56.8–81.2)	2.53 (1.9–3.3)	0.34 (0.2–0.7)	55.0 (38.5–70.7)	85.7 (72.6–94.1)

CI: 95% confidence interval, PLR: positive likelihood ratio, NLR: negative likelihood ratio, PPV: positive predictive value, NPV: negative predictive value, OCA1: outer circumpapillary annulus of circular grid 1, OCA2: outer circumpapillary annulus of circular grid 2, OCA3: outer circumpapillary annulus of circular grid 3.

Frequency of peripapillary atrophy and impact on diagnostic accuracy in the present study population.

Table 7

	PPA present				Percentage of Normals with a False Positive Diagnosis of Glaucoma				Percentage of Glaucoma Patients with a False Negative Diagnosis of Glaucoma			
	Percentage of subjects	Number of subjects	Normal	POAG	PPA absent	PPA present	P value*	P	PPA absent	PPA present	P value [†]	P
OCA1												
Superior	14.1%	22	7	15	21.7%	42.9%	0.345	0.345	14.9%	6.7%	0.682	0.682
Temporal	27.5%	43	10	33	17.5%	50%	0.038	0.038	30.4%	3.0%	0.002	0.002
Inferior	16.0%	25	8	17	11.9%	37.5%	0.091	0.091	6.9%	5.9%	1	1
Nasal	8.3%	13	3	10	43.8%	0.0%	0.259	0.259	12.7%	10.0%	1	1
All	16.5%	103	28	75	24.2%	39.3%	0.108	0.108	15.3%	5.3%	0.021	0.021
OCA2												
Superior	7.1%	11	3	8	14.1%	0.0%	1	1	24.7%	12.5%	0.675	0.675
Temporal	16.0%	25	6	19	21.3%	50%	0.142	0.142	25.7%	5.3%	0.063	0.063
Inferior	6.4%	10	3	7	12.5%	0.0%	1	1	9.8%	28.6%	0.176	0.176
Nasal	4.5%	7	2	5	38.5%	0.0%	0.525	0.525	20.2%	40.0%	0.289	0.289
All	8.5%	53	14	39	21.7%	21.4%	1	1	19.9%	15.4%	0.668	0.668

PPA: peripapillary atrophy, POAG: primary open angle glaucoma. OCA1: outer circumferential annulus of circular grid 1, OCA2: outer circumferential annulus of circular grid 2.

* p values comparing rates of a false positive diagnosis between subjects with and without PPA

† p values comparing rates of a false negative diagnosis between subjects with and without PPA